RESEARCH ARTICLE

Colossal Anisotropic Thermal Expansion in a Diazo-Functionalized Compound with Switchable Solid-State Behavior

Xiaodan Ding,[a] Daniel K. Unruh,[a] Liulei Ma,[a] Evan J. van Aalst,[a] Eric W. Reinheimer,[b] Benjamin J. Wylie,[a] and Kristin M. Hutchins*[a]

[a] X. Ding, Dr. D. K. Unruh, L. Ma, E. J. van Aalst, Prof. Dr. B. J. Wylie, Prof. Dr. K. M. Hutchins
Department of Chemistry and Biochemistry
Texas Tech University
Lubbock, Texas, 79409, United States
E-mail: kristin.hutchins@ttu.edu
[b] Dr. E. W. Reinheimer
Rigaku Americas Corporation
9009 New Trails Drive, The Woodlands, Texas, 77381, United States.

Supporting information for this article is given via a link at the end of the document.

Abstract: Achieving substantial anisotropic thermal expansion (TE) in solid-state materials is challenging as most materials undergo volumetric expansion upon heating. Here, we describe colossal, anisotropic TE in crystals of an organic compound functionalized with two azo groups. Interestingly, the material exhibits distinct and switchable TE behaviors within different temperature regions. At high temperature, two-dimensional, area zero TE and colossal, positive linear TE (α = 211 MK^{-1}) are attained due to dynamic motion, while at low temperature, moderate positive TE occurs in all directions. Investigation of the solid-state motion showed the change in enthalpy and entropy are quite different in the two temperature regions and solid-state NMR experiments support motion in the solid. Cycling experiments demonstrate that the solid-state motions and TE behaviors are completely reversible. These results reveal strategies for designing significant anisotropic and switchable behaviors in solid-state materials.

Introduction

The thermal expansion (TE) behavior of a material describes how it responds to a change in temperature.[1] Most materials experience positive TE (PTE), which involves elongation along all three principal axes upon heating.[2] Negative TE (NTE) is less common and corresponds to a decrease of the corresponding dimension upon warming.[3] Zero TE (ZTE) is rare, and the material dimension undergoes nearly no change as a function of temperature.[4] Colossal TE in materials has been defined as those that exhibit TE coefficients greater than 100 MK^{-1}, while coefficients of *ca.* 20 MK^{-1} are common in materials.[5]

Solid materials with high symmetry undergo approximately equal amounts of expansion in all directions, i.e., isotropic TE.[6] Some materials exhibit anisotropic TE, wherein significantly different expansion occurs along only one of the individual directions.[7] Such anisotropic expansion has been attained in metal-organic frameworks by designing flexible structures with wine-rack or hinge-like style frameworks, where expansion in one direction is coupled with contraction in another.[8] However, colossal anisotropic TE has been less reported in purely organic materials, especially single-component organic solids.[7a, 9] Recently, π-stacking interactions were used to attain anisotropic TE in a naphthalenediimide-based compound.[10] Materials exhibiting unique behaviors including NTE, ZTE, large PTE, or anisotropic TE are interesting and can be utilized to construct devices. For example, anisotropic expansion in materials has successfully been used to fabricate thermomechanical devices.[11] Moreover, understanding TE at the molecular level provides a pathway for controlling and affecting anisotropic behaviors within solid-state materials.

In addition to structural flexibility, molecular rotations and reorientations that occur in the solid state have also been used to achieve significant changes in cell lengths and anisotropic TE.[12] One specific type of solid-state motion, pedal motion, occurs when there is interconversion between molecular conformations (Figure 1a).[13] Olefin (C=C) and azo (N=N) functional groups are the most widely studied groups capable of facilitating molecular pedal motion in the solid state.[13c] Occurrence of pedal motion can be characterized by variable temperature single-crystal X-ray diffraction (VT SCXRD) or solid-state NMR experiments. In VT SCXRD, the motion is observed via a disorder, and the site occupancies for the two conformations (major and minor sites) are quantified in the structure. If the site occupancies undergo a change with a change in temperature, then the motion is dynamic. Our group and others have demonstrated that dynamic motion can afford large PTE in solid-state materials.[7a, 14] Such conformational interconversions, as well as phase transitions, have also been shown to yield macroscopic motion (walking, rolling) in single crystals.[15] Solids containing multiple functional groups have also been shown to exhibit collective molecular rotations, translations, and tilts, to function as molecular machines.[16]

Recently, we described a series of di-halogenated compounds wherein the degree of solid-state pedal motion was influenced by the identity of the functional group bridging the aromatic rings (olefin, imine, or azo) and larger TE occurred along the direction where motion happened in the solids.[17] In the previous study, one compound, 1,4-bis((*E*)-(4-iodophenyl)diazenyl)benzene (**diazo-I**, Figure 1b), underwent pedal motion, as well as a conformational switch in the major site orientation within one of the two crystallographically unique molecules between 250 and 270 K. Upon further investigation after that study, we determined that the β angle of the unit cell

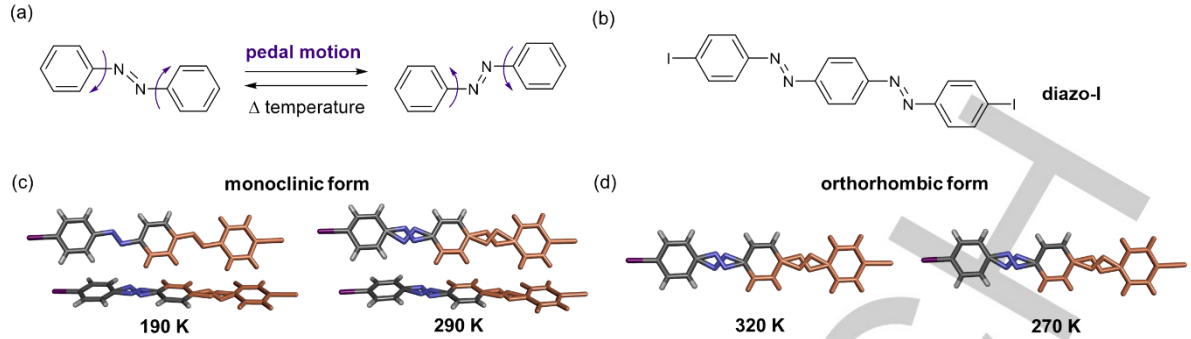

Figure 1. (a) Pedal motion in azobenzene. (b) Chemical structure of **diazo-I**. Comparison of crystallographically unique molecules and disorder in **diazo-I** for (c) monoclinic form (previous study) and (d) orthorhombic form (this study). The disorder is only shown in the azo groups for clarity. Crystallographically unique atoms are colored in orange within each molecule.

also began approaching 90° upon heating, which could result in a space group change. Thus, we sought a more detailed investigation into the solid-state behavior of **diazo-I**.

Here, we report that **diazo-I** exhibits temperature-dependent, switchable TE behavior with distinct responses at high and low temperature. At high temperature, **diazo-I** undergoes colossal, linear PTE coupled with two-dimensional (2D), area ZTE. Conversely, at low temperature, **diazo-I** undergoes minimal to moderate PTE in all three dimensions. Upon heating (~270 K and above), **diazo-I** undergoes a phase transition that involves flipping of N=N bond orientations such that all neighboring molecules lie parallel. The transition also results in an increase in symmetry, and the two crystallographically unique molecules become one with simultaneous coalescence of pedal motion via site occupancy convergence. Upon cooling below 270 K, symmetry is lost as the N=N bonds switch to an antiparallel arrangement, the site occupancies diverge, and pedal motion ceases at approximately 200 K. The transition and TE behaviors in each temperature region are reversible as demonstrated through cycling experiments. Variable-temperature solid-state NMR experiments also support the phase transition. The colossal, anisotropic TE in **diazo-I** is on par with or higher than some of the highest reported TE coefficients for single-component organic solids. Distinct behaviors over different temperature ranges in solid-state materials are desirable for applications in temperature sensing,[18] shape memory,[19] and soft robotics.[20]

Results and Discussion

Structural Transition of Diazo-I

In our previous study, VT SCXRD data was collected by mounting the crystal at 190 K and warming to 290 K while collecting data every 20 K. The structure of **diazo-I** was solved in the monoclinic space group $P2_1/c$ at each temperature, and one-half of two unique molecules were present in the asymmetric unit. One unique molecule underwent dynamic motion over the entire temperature range, while the disorder in the second molecule was only observed at higher temperatures (270 K and 290 K, Figure 1c). Importantly, the occupancies of major sites in the two molecules were nearly identical at 290 K, indicating possible convergence at a higher temperature.

Here, we synthesized **diazo-I** as reported and single crystals were grown by slow evaporation from toluene.[17] To investigate the possible convergence at high temperature, we conducted a VT SCXRD experiment by mounting the crystal at 320 K followed by cooling gradually to 270 K in 10 K increments (Table S1-S2).[21]

At 320 K, single-crystal analysis revealed **diazo-I** to lie in the orthorhombic space group *Pccn*. The asymmetric unit only contains one-half of one **diazo-I** molecule, and the molecule is disordered at 320 K (Figure 1d). Thus, at high temperature, the two unique molecules did converge to one. Upon cooling to collect additional data, **diazo-I** remains in the orthorhombic space group until 270 K. At 270 K, it appeared that the crystal was in a transition state between space groups and could be reasonably solved in either an orthorhombic or monoclinic crystal system due to the ambiguity of the systematic absence violations (Table S2). Additional data was collected at 260 K, which showed **diazo-I** transitioned to the low temperature, monoclinic phase (Table S2).

Solid-State Structure and Motion

In the solid state, **diazo-I** self-assembles into a 2D halogen-bonded sheet through type II I···I halogen bonds that lie in the *ac* plane (Figure 2a). Along the *b* axis, the sheets pack into herringbone π-stacked layers through type I I···I, C-H···π, and C-H···I interactions (Figure 2b). Between 320-270 K, **diazo-I** undergoes dynamic pedal motion as confirmed by small changes in the site occupancies (Table 1). For consistency in modeling the disorder within each structure, the same constraints and restraints

Table 1. Occupancies of the major site conformation within **diazo-I** obtained from the VT SCXRD data. The minor site occupancy is equal to 1 – the major site. The error is shown in parentheses.

Temperature [K]	Major site occupancy
320	0.70(1)
310	0.72(1)
300	0.72(1)
290	0.74(1)
280	0.75(1)
270	0.79(1)[a]

[a] The value obtained is from structure solution in the orthorhombic space group.

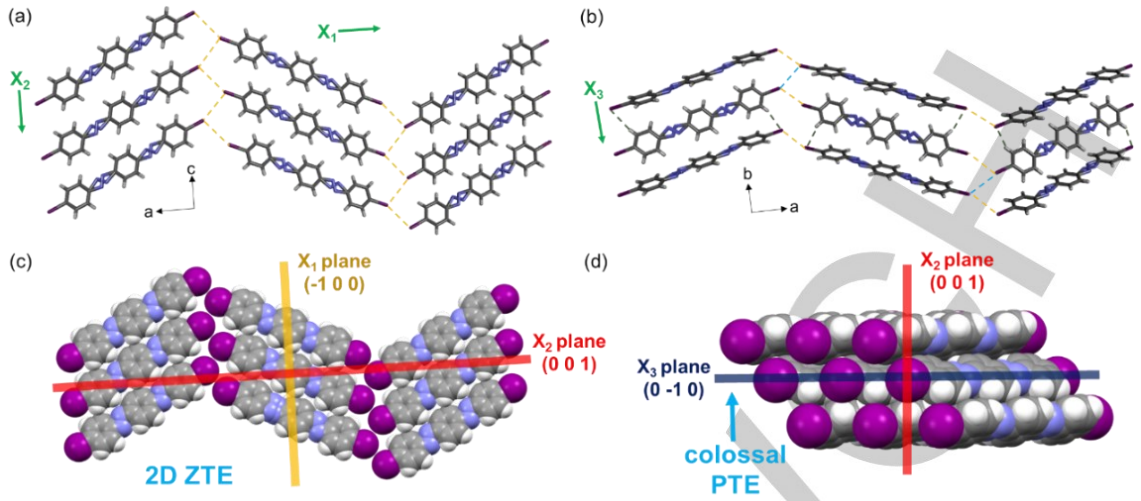

Figure 2. Single-crystal X-ray structures of **diazo-I** at 280 K: (a, b) 2D halogen-bonded sheets, layers, and TE axes. (c, d) The principal axes, X_1, X_2, and X_3 of TE (all planes are going into the page). Dashed lines indicate intermolecular interactions: type II I···I bonds (yellow), type I I···I bonds (blue), and C-H···I forces (green). The disorder is only shown in the azo groups for clarity.

were applied at each temperature while allowing the sites to freely refine.

Using the VT SCXRD data, the conformational interconversion between the two sites (i.e. pedal motion) was further investigated through a van't Hoff analysis. The natural logarithm of the ratio of the major and minor site conformations is plotted against the reciprocal of temperature.[13a, 22] The data is approximately linear from 320-280 K; however the data deviates from linearity at 270 K due to reaching the tipping point of the space group change (Figure 3). The linearity from 320-280 K indicates that the pedal motion reaches thermodynamic equilibrium and the entropic and enthalpic differences between the two sites are constant. The enthalpy and entropy differences between the two conformations were calculated using the van't Hoff equation:

$$\ln\frac{[major\ site]}{[minor\ site]} = -\frac{\Delta H}{RT} + \frac{\Delta S}{R} \qquad [1]$$

The slope is equal to -ΔH/R, and the intercept is equal to ΔS/R. Using equation 1 and the linear fit from 320-280 K (Figure 3), ΔH = -4.5 kJ mol^{-1} and ΔS = -6.9 J K^{-1} mol^{-1}. The conformational

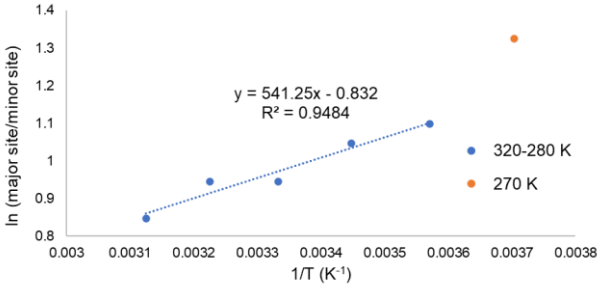

Figure 3. The van't Hoff plot for **diazo-I** including temperature data from 320-270 K. The linear fit is only applied to the data points from 320-280 K.

change is an exothermic process, and the change in enthalpy is similar in magnitude to formation of a hydrogen bond. The change in entropy is negative because the system becomes more ordered upon cooling when the population of the major conformation increases. It is also of interest to note that **diazo-I** is a symmetric molecule, and symmetry has been shown to affect barriers to molecular motion.[16b, 16c]

Thermal Expansion Behavior

The program PASCal[23] was used to calculate the principal axes of TE (X_1, X_2, and X_3) and coefficients of TE (α) using the VT SCXRD data from 320-280 K (Table S6, Figure S2).

Analysis of the unit cell parameters of **diazo-I** demonstrates that the *a* axis expands on cooling (NTE), while the *b* and *c* axes contract on cooling (PTE, Figure 4). From 320-280 K, **diazo-I** undergoes appreciable NTE along principal axis X_1 coupled with nearly equal PTE along principal axis X_2. The coefficient of TE along the X_1 axis is -65(1) MK^{-1} and corresponds to the crystallographic *a* axis. The coefficient of TE along the X_2 axis is 64(3) MK^{-1} and corresponds to the crystallographic *c* axis. The X_1 axis encompasses the longer width of the molecule, while the X_2 axis lies along the shorter width of the molecule. Together, the X_1 and X_2 axes encompass the 2D halogen-bonded sheet (Figure 2c). Thus, **diazo-I** undergoes 2D area ZTE within the halogen-bonded sheet due to the TE coefficients being equal, but opposite in sign. The I···I halogen bonds contribute to TE along X_1 and X_2, which decrease in length by 0.01 Å upon cooling (Figure 2a, Table S7-S8). The TE behavior along X_1 and X_2 is also explained by the influence of molecular width, indicating that the direction of larger width experiences less expansion.[24]

Extremely colossal and linear PTE occurs along principal axis X_3, and the coefficient of TE is 211(2) MK^{-1}. The X_3 axis corresponds to the crystallographic *b* axis, and includes the herringbone π-stacked layers (Figure 2d). The molecules along the π-stacked layers are oriented in an edge-to-face arrangement.

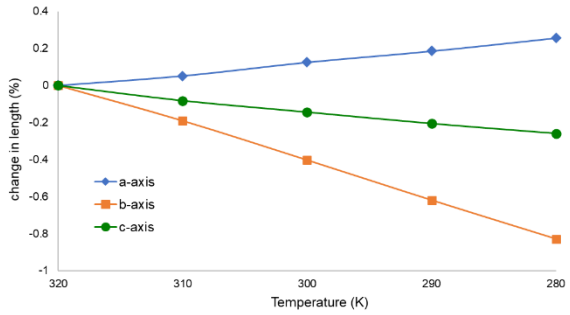

Figure 4. Percent change in length of the unit cell axes as a function of temperature for **diazo-I**. The change is calculated based on the values at 320 K. A decrease on cooling corresponds to PTE.

The dynamic interconversion between the two molecular conformations *(i.e.*, pedal motion) of **diazo-I** affects both X_2 and X_3 due to the herringbone packing arrangement and contributes to the colossal PTE along X_3. The volumetric TE coefficient (210(2) MK^{-1}) is nearly equal to the X_3 coefficient due to the occurrence of 2D area ZTE. Although the TE could not be observed macroscopically (Figure S3-S4), the TE along X_3 in **diazo-I** is on par with or higher than some of the highest reported TE coefficients for single-component organic solids (Table S13).

Reversibility in the Transition for Diazo-I

To investigate the full solid-state behavioral profile and reversibility in the phase transition of **diazo-I**, we conducted a cycling VT SCXRD experiment by cooling from 320-100 K and then warming back to 320 K while collecting full crystallographic data sets every 10 K. A total of 45 full data sets were collected on one single crystal (Table S4). Upon cooling, the β angle clearly begins to deviate from 90° near 270 K (Figure 5), indicating the occurrence of the space group transition.

During both the cooling and heating portions of the cycle, **diazo-I** lies in the orthorhombic space group from 320-280 K and in the monoclinic space group from 260-100 K (Figure 5). In the orthorhombic system, one-half of one unique molecule of **diazo-I** is present, and in the monoclinic system, one-half of two unique molecules are present. At high temperatures, **diazo-I** undergoes pedal motion, while at low temperatures, only one of the two unique molecules undergoes pedal motion, and motion ceases at *ca.* 200 K.

Inspection of the structures above and below the transition provides key insight into what occurred. At high temperature, every molecule is identical and neighboring molecules within the herringbone π-stacks lie parallel (see major site conformations, Figure S8). Upon cooling below the phase transition temperature, symmetry is lost as the site occupancies diverge. The ordered molecule remains in the same conformation as it is at high temperature; however, the disordered molecule flips conformation such that neighboring **diazo-I** molecules within the herringbone π-stacks now lie antiparallel to each other (Figure S8). This antiparallel arrangement persists upon cooling to 100 K. The angle between neighboring molecules in the herringbone π-stacks also undergoes a dramatic switch at the phase change. Upon cooling from 320-280 K, the molecules twist toward being more coplanar by *ca.* 1.3°, but during the phase change, the molecules twist back to the original orientation seen at 320 K (Figure S9).

A van't Hoff analysis was performed using the VT SCXRD data for all four regions of the cycling experiment (Table 2, Figure S13-S16). For the first cooling portion, the plot is linear in the range of 320-280 K and the 270 data deviates from the linearity, which is identical to the conclusion from the first experiment (see Figure 3). The values of ΔH and ΔS are also similar to the first experiment (Table 2). In the second half of the cooling portion, the van't Hoff plot is linear from 260-210 K, and motion ceases at 200 K. The change in enthalpy and entropy over the lower temperature range are significantly different than the higher temperature range of the cycle. The overall change in the site occupancies is also much larger within the low temperature range when compared to the high temperature range (30% vs. 5%).

In the heating portion of the cycle, pedal motion begins at 200 K and the crystal remains in the monoclinic space group until 260 K. Upon reaching approximately 270 K, the space group switches from monoclinic to orthorhombic, the site occupancies re-converge, and **diazo-I** undergoes pedal motion from 270-320 K.

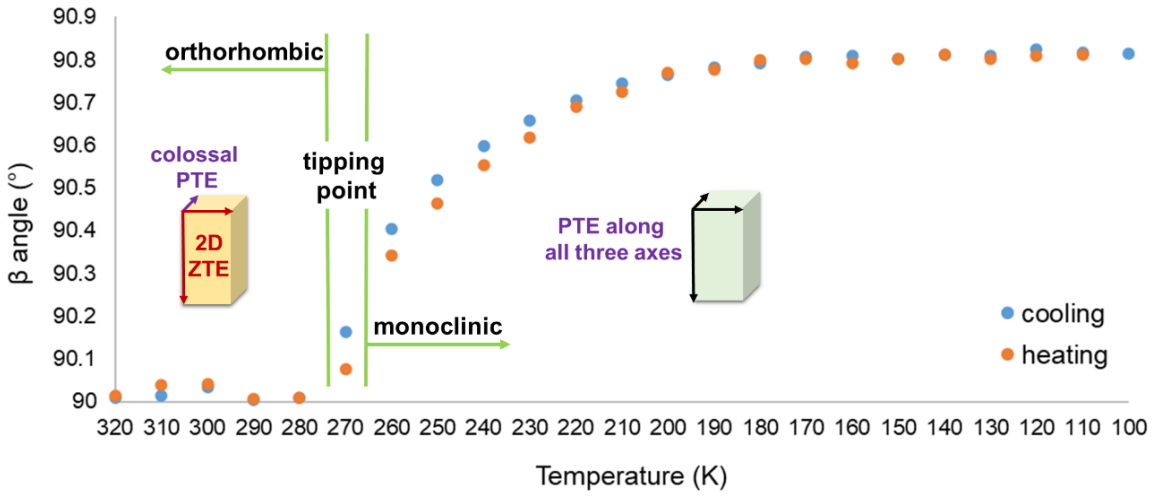

Figure 5. The β angle in **diazo-I** as a function of temperature for the cycling experiment and differences in TE behavior within the two regions. Cooling from 320-100 K is shown with blue markers and heating back to 320 K is shown with orange markers.

Table 2. Total site occupancy changes over a given temperature range, and enthalpic and entropic parameters obtained from linear fitting of van't Hoff plots from Figures 2, S14, and S16.

Temperature range [K]	Experiment	Site occupancy change over range	ΔH [kJ mol^{-1}]	ΔS [J K-1 mol^{-1}]
320-280	High temperature region	5%	-4.5	-6.9
320-280	Cycling (cooling)	5%	-4.7	-8.4
	Cycling (heating)	6%	-5.4	-11.0
260-210	Cycling (cooling)	31%	-16.3	-57.9
200-260	Cycling (heating)	38%	-16.8	-61.0

It is important to note that different crystals were used for the initial 320-270 K experiment and the cycling experiment. Although there are sources of error in the modeling of each X-ray structure, the refined site occupancies and ΔH values are quite similar between crystals.

Solid-State Dynamics

As **diazo-I** undergoes solid-state motion, the position of the nitrogen atoms within the major site conformation allows for a C-H···N interaction to form with an aromatic ring in a neighboring diazo molecule (Figure S10). Thus, as the population of the major conformation increases upon cooling, C-H···N interactions can form. At the phase transition, the conformational switch in the azo group orientations also afford shorter C-H···N interactions between neighboring π-stacked **diazo-I** molecules (Figure S11). The significant difference in site occupancy changes (Table 2) and intermolecular forces contributes to the large differences in enthalpy and entropy above and below the transition.

Magic-angle spinning (MAS) ^{13}C solid-state NMR (SSNMR) experiments were conducted to further investigate the phase change. Indeed, between ca. 270-260 K additional signals in the aromatic region appeared in addition to significant shifting of the signals corresponding to the carbons adjacent to the azo groups (Figure 6, Figure S17-S18). The changes were observed using MAS rates of both 8 kHz and 20 kHz. The carbon atoms that exhibit the most significant changes are those that engage in the C-H···N interactions upon cooling (C3 and C5, Figure 6). Differential scanning calorimetry was performed and showed a small, discernible transition (Figure S19).

Switchable Thermal Expansion

Perhaps of most interest, the TE behavior of **diazo-I** is switchable during the cycling experiment (Table S10). Using the 45 data sets obtained from the cycling experiment, the TE values were calculated for each portion of the cycle. Above 270 K, on both the cooling and heating portions of the cycle, **diazo-I** exhibits 2D area ZTE in the *ac* plane and colossal, linear PTE along the *b* axis with coefficients of *ca.* 215 MK^{-1}. This behavior is identical to the TE discussed above in the non-cycling experiment. From 260-100 K on both the cooling and heating parts of the cycle, **diazo-I** experiences mild to large PTE along all three crystallographic axes (α = 24, 47, and *ca.* 100 MK^{-1}), a significantly more common behavior in organic materials. **Diazo-I** exhibits distinct and reversible TE behavior, depending on which temperature and phase the material lies in. Overall, **diazo-I** exhibits a unique combination of solid-state behaviors in response to temperature (Figure 7).

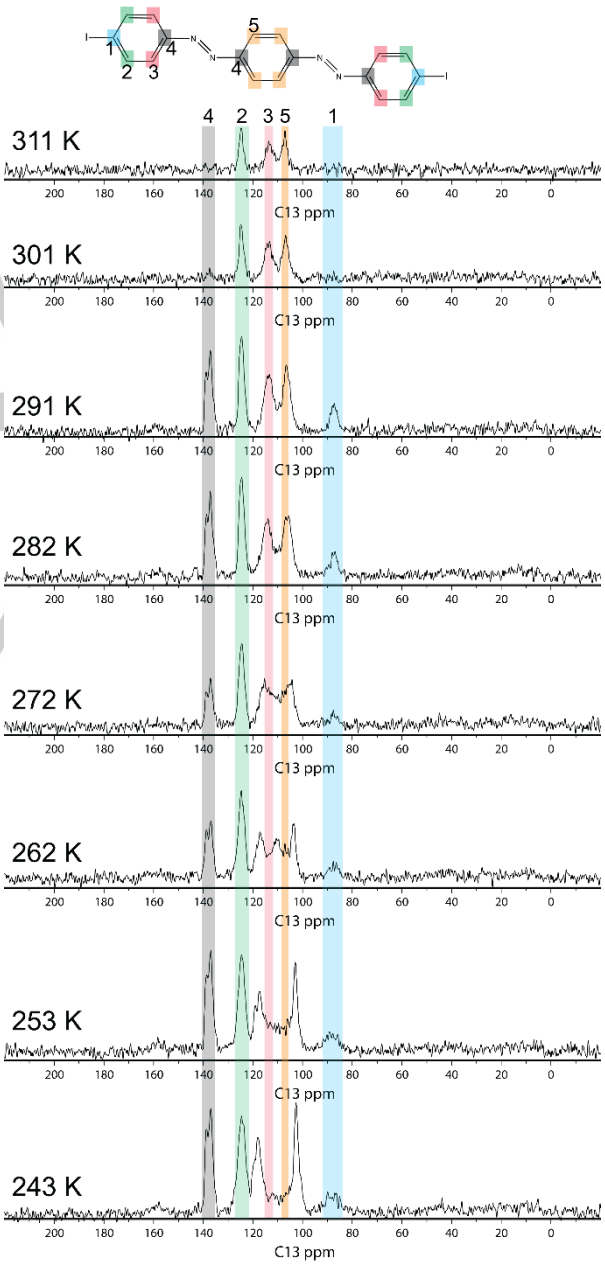

Figure 6. ^{13}C MAS SSNMR data for **diazo-I** using a MAS rate of 20 kHz. The sample temperature is noted on each spectrum.

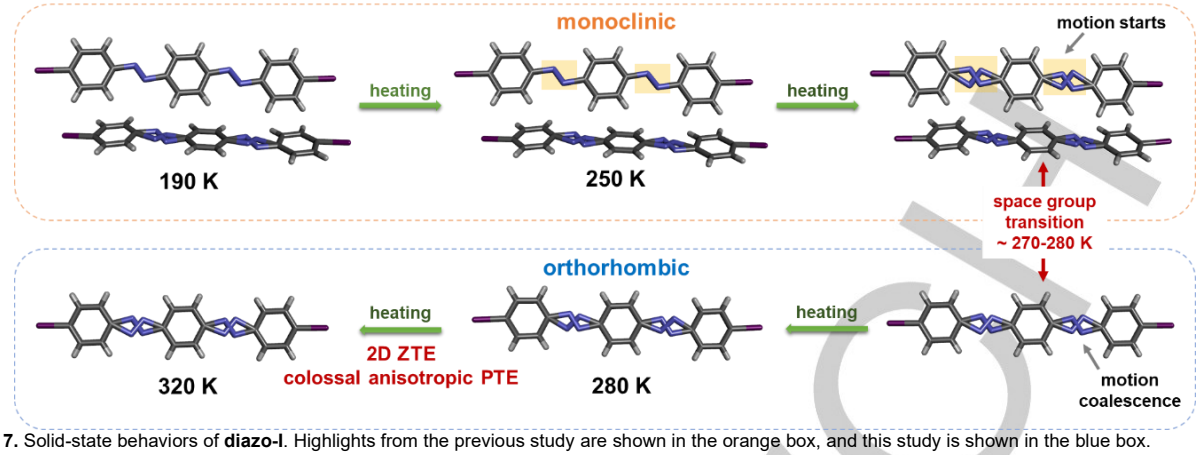

Figure 7. Solid-state behaviors of **diazo-I**. Highlights from the previous study are shown in the orange box, and this study is shown in the blue box.

We expect that the behaviors seen here in **diazo-I** can be used in designing anisotropic and switchable solid-state properties. Use of functional groups that undergo dynamic motion aids in attaining large TE in organic materials. However, TE can be limited or switched by facilitating the formation of favorable intermolecular forces to strengthen a given direction within the solid and limit the TE.

Conclusion

In summary, we investigated the detailed solid-state thermal expansion and dynamic behavior of **diazo-I**. **Diazo-I** experiences common, positive TE along all three axes at low temperature, but at high temperature, rare 2D area zero TE coupled with colossal, linear positive TE occurs. A van't Hoff analysis provided insight into the thermodynamics of the solid-state motion, which differs significantly in the high and low temperature regions. In both regions, the enthalpic differences correspond to formation of intermolecular hydrogen bonds, but the conformational interconversion is larger in the low temperature region and the hydrogen bonds become much shorter. SSNMR also supports the motion and transition in **diazo-I**. The solid-state properties exhibited by **diazo-I** are advantageous for design of thermomechanical sensors, and we are continuing to study anisotropic behaviors and TE in organic materials.

Acknowledgements

K.M.H. gratefully acknowledges financial support from the National Science Foundation (DMR-2045506). The authors acknowledge Professor Michael Latham for valuable conversations.

Conflict of Interest

The authors declare no conflicts of interest.

Keywords: anisotropic thermal expansion • azo compounds • crystal engineering • solid-state motion • switchable behaviors

[1] a) Y. Zhang, B. Chen, D. Guan, M. Xu, R. Ran, M. Ni, W. Zhou, R. O'Hayre, Z. Shao, *Nature* **2021**, *591*, 246-251; b) V. A. Drebushchak, *J. Therm. Anal. Calorim.* **2020**, *142*, 1097-1113; c) Q.-F. Guan, H.-B. Yang, Z.-M. Han, L.-C. Zhou, Y.-B. Zhu, Z.-C. Ling, H.-B. Jiang, P.-F. Wang, T. Ma, H.-A. Wu, S.-H. Yu, *Sci. Adv.* **2020**, *6*, eaaz1114; d) B. K. Saha, *J. Indian Inst. Sci.* **2017**, *97*, 177-191.

[2] a) X. Guo, X. Ni, J. Li, H. Zhang, F. Zhang, H. Yu, J. Wu, Y. Bai, H. Lei, Y. Huang, J. A. Rogers, Y. Zhang, *Adv. Mater.* **2021**, *33*, 2004919; b) N. Juneja, E. Zahid, D. K. Unruh, K. M. Hutchins, *CrystEngComm* **2021**, *23*, 4439-4443; c) D. H. Fabini, C. C. Stoumpos, G. Laurita, A. Kaltzoglou, A. G. Kontos, P. Falaras, M. G. Kanatzidis, R. Seshadri, *Angew. Chem. Int. Ed.* **2016**, *128*, 15618-15622.

[3] a) N. Shi, A. Sanson, Q. Sun, L. Fan, A. Venier, D. Oliveira de Souza, X. Xing, J. Chen, *Chem. Mater.* **2021**, *33*, 1321-1329; b) Z. Liu, Q. Gao, J. Chen, J. Deng, K. Lin, X. Xing, *Chem. Commun.* **2018**, *54*, 5164-5176; c) Q. Li, K. Lin, Z. Liu, L. Hu, Y. Cao, J. Chen, X. Xing, *Chem. Rev.* **2022**, *122*, 8438-8486; d) N. C. Burtch, S. J. Baxter, J. Heinen, A. Bird, A. Schneemann, D. Dubbeldam, A. P. Wilkinson, *Adv. Funct. Mater.* **2019**, *29*, 1904669.

[4] a) J. R. Salvador, F. Guo, T. Hogan, M. G. Kanatzidis, *Nature* **2003**, *425*, 702-705; b) Z. Ren, R. Zhao, X. Chen, M. Li, X. Li, H. Tian, Z. Zhang, G. Han, *Nat. Commun.* **2018**, *9*, 1638; c) Z.-Y. Zou, Y.-H. Lou, X.-Q. Song, H. Jiang, K. Du, C.-Z. Yin, W.-Z. Lu, X.-C. Wang, X.-H. Wang, M. Fu, W. Lei, *Adv. Mater. Interf.* **2021**, *8*, 2100584.

[5] A. L. Goodwin, M. Calleja, M. J. Conterio, M. T. Dove, J. S. O. Evans, D. A. Keen, L. Peters, M. G. Tucker, *Science* **2008**, *319*, 794-797.

[6] a) X.-L. Peng, S. Bargmann, *Extreme Mech. Lett.* **2021**, *43*, 101201; b) Q. Gao, J. Wang, A. Sanson, Q. Sun, E. Liang, X. Xing, J. Chen, *J. Am. Chem. Soc.* **2020**, *142*, 6935-6939; c) L. Wu, B. Li, J. Zhou, *ACS Appl. Mater. Interfaces* **2016**, *8*, 17721-17727.

[7] a) D. Das, T. Jacobs, L. J. Barbour, *Nat. Mater.* **2010**, *9*, 36-39; b) I. Grobler, V. J. Smith, P. M. Bhatt, S. A. Herbert, L. J. Barbour, *J. Am. Chem. Soc.* **2013**, *135*, 6411-6414; c) A. D. Fortes, E. Suard, K. S. Knight, *Science* **2011**, *331*, 742-746.

[8] a) S. Henke, A. Schneemann, R. A. Fischer, *Adv. Funct. Mater.* **2013**, *23*, 5990-5996; b) L. Zhang, X. Kuang, X. Wu, W. Yang, C. Lu, *Dalton Trans.* **2014**, *43*, 7146-7152; c) L. D. DeVries, P. M. Barron, E. P. Hurley, C. Hu, W. Choe, *J. Am. Chem. Soc.* **2011**, *133*, 14848-14851.

[9] a) S. Dutta, P. Munshi, *J. Phys. Chem. C* **2020**, *124*, 27413-27421; b) D. Das, L. J. Barbour, *CrystEngComm* **2018**, *20*, 5123-5126; c) A. Janiak, C. Esterhuysen, L. J. Barbour, *Chem. Commun.* **2018**, *54*, 3727-3730; d) L. O. Alimi, D. P. van Heerden, P. Lama, V. J. Smith, L. J. Barbour, *Chem. Commun.* **2018**, *54*, 6208-6211.

[10] M. Dharmarwardana, B. M. Otten, M. M. Ghimire, B. S. Arimilli, C. M. Williams, S. Boateng, Z. Lu, G. T. McCandless, J. J. Gassensmith, M. A. Omary, *PNAS* **2021**, *118*, e2106572118.

[11] a) M. Jin, S. Yamamoto, T. Seki, H. Ito, M. A. Garcia-Garibay, *Angew. Chem. Int. Ed.* **2019**, *58*, 18003-18010; b) P. Naumov, S. Chizhik, M. K. Panda, N. K. Nath, E. Boldyreva, *Chem. Rev.* **2015**, *115*, 12440-12490; c) S. C. Sahoo, M. K. Panda, N. K. Nath, P. Naumov, *J. Am. Chem. Soc.* **2013**, *135*, 12241-12251; d) P. Gupta, D. P. Karothu, E. Ahmed, P. Naumov, N. K. Nath, *Angew. Chem. Int. Ed.* **2018**, *130*, 8634-8638.

[12] a) Z.-S. Yao, H. Guan, Y. Shiota, C.-T. He, X.-L. Wang, S.-Q. Wu, X. Zheng, S.-Q. Su, K. Yoshizawa, X. Kong, *Nat. Commun.* **2019**, *10*, 4805; b) Z.-S. Yao, M. Mito, T. Kamachi, Y. Shiota, K. Yoshizawa, N. Azuma, Y. Miyazaki, K. Takahashi, K. Zhang, T. Nakanishi, S. Kang, S. Kanegawa, O. Sato, *Nat. Chem.* **2014**, *6*, 1079-1083; c) Z.-S. Yao, Z. Tang, J. Tao, *Chem. Commun.* **2020**, *56*, 2071-2086; d) X.-L. Wang, J.-P. Xue, X.-P. Sun, Y.-X. Zhao, S.-Q. Wu, Z.-S. Yao, J. Tao, *Chem. Eur. J.* **2020**, *26*, 6778-6783; e) E. Ahmed, D. P. Karothu, A. Slimani, J. Mahmoud Halabi, I. Tahir, K. Q. Canales, P. Naumov, *Adv. Funct. Mater.* **2022**, *32*, 2112117.

[13] a) J. Harada, K. Ogawa, *Chem. Soc. Rev.* **2009**, *38*, 2244-2252; b) J. Harada, M. Harakawa, K. Ogawa, *Acta Cryst. B* **2004**, *60*, 589-597; c) J. Harada, K. Ogawa, *J. Am. Chem. Soc.* **2001**, *123*, 10884-10888.

[14] a) N. Juneja, D. K. Unruh, E. Bosch, R. H. Groeneman, K. M. Hutchins, *New J. Chem.* **2019**, *43*, 18433-18436; b) X. Ding, D. K. Unruh, R. H. Groeneman, K. M. Hutchins, *Chem. Sci.* **2020**, *11*, 7701-7707; c) N. Juneja, N. M. Shapiro, D. K. Unruh, E. Bosch, R. H. Groeneman, K. M. Hutchins, *Angew. Chem. Int. Ed.* **2022**, *61*, e202202708; d) K. M. Hutchins, D. K. Unruh, F. A. Verdu, R. H. Groeneman, *Cryst. Growth Des.* **2018**, *18*, 566-570; e) S. Scherb, A. Hinaut, R. Pawlak, J. G. Vilhena, Y. Liu, S. Freund, Z. Liu, X. Feng, K. Müllen, T. Glatzel, A. Narita, E. Meyer, *Commun. Mater.* **2020**, *1*, 8; f) B. Dwivedi, A. Shrivastava, L. Negi, D. Das, *Cryst. Growth Des.* **2019**, *19*, 2519-2524; g) P. Commins, I. T. Desta, D. P. Karothu, M. K. Panda, P. Naumov, *Chem. Commun.* **2016**, *52*, 13941-13954.

[15] a) T. Taniguchi, H. Sugiyama, H. Uekusa, M. Shiro, T. Asahi, H. Koshima, *Nat. Commun.* **2018**, *9*, 538; b) T. Taniguchi, T. Asahi, H. Koshima, *Crystals* **2019**, *9*, 437.

[16] a) A. N. Sokolov, D. C. Swenson, L. R. MacGillivray, *PNAS* **2008**, *105*, 1794-1797; b) T.-A. V. Khuong, J. E. Nuñez, C. E. Godinez, M. A. Garcia-Garibay, *Acc. Chem. Res.* **2006**, *39*, 413-422; c) P. D. Jarowski, K. N. Houk, M. A. Garcia-Garibay, *J. Am. Chem. Soc.* **2007**, *129*, 3110-3117.

[17] X. Ding, E. Zahid, D. K. Unruh, K. M. Hutchins, *IUCrJ* **2022**, *9*, 31-42.

[18] S. K. Park, Y. Diao, *Chem. Soc. Rev.* **2020**, *49*, 8287-8314.

[19] a) K. Bhattacharya, S. Conti, G. Zanzotto, J. Zimmer, *Nature* **2004**, *428*, 55-59; b) B. B. Rath, G. Gallo, R. E. Dinnebier, J. J. Vittal, *J. Am. Chem. Soc.* **2021**, *143*, 2088-2096; c) H. Chung, D. Dudenko, F. Zhang, G. D'Avino, C. Ruzié, A. Richard, G. Schweicher, J. Cornil, D. Beljonne, Y. Geerts, Y. Diao, *Nat. Commun.* **2018**, *9*, 278.

[20] A. Miriyev, K. Stack, H. Lipson, *Nat. Commun.* **2017**, *8*, 596.

[21] CCDC Deposition Numbers 2170086, 2170087, 2170088, 2170089, 2170090, 2170091, and 2170092 contain the supplementary crystallographic data for this paper. These data are provided free of charge by the Cambridge Crystallographic Data Centre.

[22] a) C. M. L. Vande Velde, A. Collas, R. De Borger, F. Blockhuys, *Chem. Eur. J.* **2011**, *17*, 912-919; b) J. Harada, K. Ogawa, *J. Am. Chem. Soc.* **2004**, *126*, 3539-3544.

[23] M. J. Cliffe, A. L. Goodwin, *J. Appl. Crystallogr.* **2012**, *45*, 1321-1329.

[24] S. A. Rather, V. G. Saraswatula, D. Sharada, B. K. Saha, *New J. Chem.* **2019**, *43*, 17146-17150.

Entry for the Table of Contents

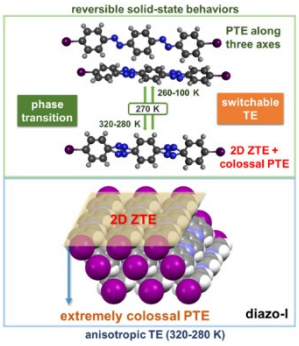

The switchable solid-state behavior of **diazo-I** is described. Dramatically different and fully reversible thermal expansion (TE) behaviors are obtained on either side of a phase transition. Moderate, positive TE along all axes occurs at low temperature and two-dimensional, area zero TE coupled with colossal, positive TE occurs at high temperature.

Institute and/or researcher Twitter usernames: @KM_Hutchins